Acta Pharmaceutica Sinica B 2025;15(2):991−1006

Chinese Pharmaceutical Association
Institute of Materia Medica, Chinese Academy of Medical Sciences

Acta Pharmaceutica Sinica B

www.elsevier.com/locate/apsb
www.sciencedirect.com

ORIGINAL ARTICLE

A small molecule cryptotanshinone induces non-enzymatic NQO1-dependent necrosis in cancer cells through the JNK1/2/Iron/PARP/calcium pathway

Ying Hou[a], Bingling Zhong[a], Lin Zhao[a], Heng Wang[a], Yanyan Zhu[a], Xianzhe Wang[a], Haoyi Zheng[a], Jie Yu[a], Guokai Liu[b], Xin Wang[c], Jose M. Martin-Garcia[d], Xiuping Chen[a,e,f,*]

[a]*State Key Laboratory of Quality Research in Chinese Medicine, Institute of Chinese Medical Sciences, University of Macau, Macao 999078, China*
[b]*School of Pharmaceutical Sciences, Shenzhen University Medical School, Shenzhen University, Shenzhen 518055, China*
[c]*Faculty of Biology, Medicine and Health, the University of Manchester, Manchester M13 9PT, UK*
[d]*Department of Crystallography & Structural Biology, Institute of Physical Chemistry Blas Cabrera, Spanish National Research Council (CSIC), Madrid 28006, Spain*
[e]*MoE Frontiers Science Center for Precision Oncology, University of Macau, Macao 999078, China*
[f]*GMU-GIBH Joint School of Life Sciences, the Guangdong-Hong Kong-Macau Joint Laboratory for Cell Fate Regulation and Diseases, Guangzhou Medical University, Guangzhou 510005, China*

Received 7 May 2024; received in revised form 17 July 2024; accepted 26 July 2024

KEY WORDS

NQO1;
Cryptotanshinone;
Iron;
Ferroptosis;
NAD^+ depletion;
Calcium;
Targeted therapy;
Cancer

Abstract Human NAD(P)H: quinone oxidoreductase 1 (NQO1) is a flavoenzyme expressed at high levels in multiple solid tumors, making it an attractive target for anticancer drugs. Bioactivatable drugs targeting NQO1, such as β-lapachone (β-lap), are currently in clinical trials for the treatment of cancer. β-Lap selectively kills NQO1-positive ($NQO1^+$) cancer cells by inducing reactive oxygen species (ROS) *via* catalytic activation of NQO1. In this study, we demonstrated that cryptotanshinone (CTS), a naturally occurring compound, induces NQO1-dependent necrosis without affecting NQO1 activity. CTS selectively kills $NQO1^+$ cancer cells by inducing NQO1-dependent necrosis. Interestingly, CTS directly binds to NQO1 but does not activate its catalytic activity. In addition, CTS enables activation of JNK1/2 and PARP, accumulation of iron and Ca^{2+}, and depletion of ATP and NAD^+.

*Corresponding author.
E-mail address: xpchen@um.edu.mo (Xiuping Chen).

Peer review under the responsibility of Chinese Pharmaceutical Association and Institute of Materia Medica, Chinese Academy of Medical Sciences.

https://doi.org/10.1016/j.apsb.2024.12.005

Furthermore, CTS selectively suppressed tumor growth in the NQO1$^+$ xenograft models, which was reversed by NQO1 inhibitor and NQO1 shRNA. In conclusion, CTS induces NQO1-dependent necrosis *via* the JNK1/2/iron/PARP/NAD$^+$/Ca^{2+} signaling pathway. This study demonstrates the non-enzymatic function of NQO1 in inducing cell death and provides new avenues for the design and development of NQO1-targeted anticancer drugs.

1. Introduction

Lung cancer is the leading cause of cancer-related death worldwide[1]. Among the subtypes of lung cancer, non-small cell lung cancer (NSCLC) accounts for nearly 85% of all lung cancer patients[2]. Despite the extensive research involved in targeted therapy and immunotherapy contributing to the improvement of overall survival, effective therapies for most lung cancer patients remain unavailable[3]. Thus, exploring new targets and treatment approaches is still urgent.

The human NAD(P)H: quinone oxidoreductase 1 (NQO1; EC 1.6.5.2), also referred to as DT diaphorase in earlier literature[4], is a cytosolic multifunctional flavoenzyme that catalyzes the two-electron reduction of quinones to hydroquinones in an NAD(P)H-dependent manner[5]. NQO1 overexpression has been documented in various cancers including lung, breast, colon, pancreatic, adrenal, bladder, liver, ovarian, cervical, and thyroid, making this enzyme an attractive cancer target for drug development[6-9]. NQO1 has been found to be overexpressed up to 200-fold in more than 80% of NSCLC cases and up to 100-fold in more than 80% of pancreatic cancer cases[10]. NQO1 acts as a phase II enzyme by catalyzing the detoxification of various endogenous and exogenous toxic substances including xenobiotic quinones, such as ubiquinone, CoQ derivatives, vitamin E quinone, catechol estrogen *o*-quinones, dopamine-derived quinones, and others[11]. Several natural naphthoquinones such as β-lapachone (β-lap), BBI608, deoxynyboquinones, 2-methoxy-6-acetyl-7-methyljuglone (MAM), and tanshindiol B (TSB), have been identified as excellent NQO1 substrates[12-15]. The catalytic detoxification of these quinones to semiquinones and hydroquinone by NQO1 leads to the rapid generation of reactive oxygen species (ROS) which promotes oxidative DNA damage, activation of c-Jun N-terminal kinase 1/2 (JNK1/2), elevation of Ca^{2+}, hyperactivation of poly(ADP-ribose) polymerase-1 (PARP-1), depletion of NAD$^+$ and ATP, and ultimately, induction of cell death in NQO1$^+$ cancer cells[13,14,16,17]. These exogenous NQO1 substrates are referred to as NQO1 bioactivatable drugs (NBDs). β-Lap, the flagship NBD, is in phase I/phase II clinical trials and shows an apparent NQO1-dependent anticancer effect in human patients with refractory advanced solid tumors[18,19]. In addition, several other NBDs are being developed and tested from bench to bedside.

Tanshinones, a family of over 40 lipophilic abietane diterpenes, are extracted from *Salvia miltiorrhiza* Bunge (Danshen), a well-known Chinese herb[20]. Danshen has been used as a cardiovascular protection herb[21]. However, modern research shows that tanshinones have a wide range of pharmacological activities, such as anticancer, anti-inflammatory, and neuroprotective[22,23]. Cryptotanshinone (CTS), the second most abundant tanshinone in Danshen, exhibits diverse pharmacological effects including anticancer, anti-inflammatory, neuroprotective, and anti-fibrosis[24,25]. The anticancer effects of CTS on cancers such as lung, liver, stomach, colon, breast, bladder, ovarian, melanoma, and leukemia have been well established in the literature[24,25] while the underlying mechanisms and molecular targets are still unclear. The signal transducer and activator of transcription 3 (STAT3) has been reported as one of the candidate targets of CTS for anticancer effect[26]. We previously reported that CTS kills cancer cells by inducing pro-death autophagy through JNK1/2 signaling mediated by ROS[27]. In this study, we used the NQO1 high-expressing cell lines A549 and H460 as well as H460 xenograft models to identify NQO1 as a novel anticancer target of CTS. Furthermore, we found that CTS does not affect the catalytic activity of NQO1, in contrast to the extensively studied NBDs.

2. Materials and methods

2.1. Chemicals and reagents

CTS (purity>98%) purchased from Chengdu Pufei De Biotech Co., Ltd. was prepared as a 20 mmol/L stock solution in dimethyl sulfoxide (final concentration < 0.1% (*v*/*v*)) and stored at −20 °C. Deferoxamine (DFO), deferiprone (DFP), propidium iodide (PI), Hochest 33342, GSK'827, necrosulfonamide (NSA), and 3-[4,5-dimethylthiazol-2-yl]-2,5 diphenyl tetrazolium bromide (MTT) were purchased from Sigma−Aldrich (St. Louis, MO, USA). Dicomarol (DIC), olaparib, VX765, 2-aminoethyl diphenylborinate (2APB), BAPTA, and β-lap were purchased from Selleckchem (Houston, TX, USA). Oxidized nicotinamide adenine dinucleotide (NAD$^+$), cycloheximide (CHX), ferrostatin-1 (Fer-1), flavin adenine dinucleotide (FAD), and reduced nicotinamide adenine dinucleotide (NADH) were purchased from MedChemExpress (New Jersey, USA). DiI was purchased from Invitrogen (Carlsbad, CA, USA). 2′,7′-Dichlorofluorescin diacetate ($DCFH_2$-DA), and calcein-AM were purchased from Molecular Probes (Eugene, OR, USA). RIPA lysis buffer, phenylmethanesulfonyl fluoride (PMSF), cocktail, Coomassie blue staining solution, isopropyl-L-thio-B-D-galactopyranoside (IPTG), NAD$^+$/NADH kit, and lactate dehydrogenase (LDH) kit were purchased from Beyotime (Shanghai, China). The CellTiter-Glo® assay kit was purchased from Promega (Madison, WI, USA). Primary antibodies for NQO1, GPX4, JNK1/2, p-JNK1/2, caspase 1/3/7/8, gasdermin D (GSDMD), and poly/mono-ADP ribose (PAR) were purchased from Cell Signaling Technology (Beverly, MA, USA). GAPDH was purchased from Proteintech (Chicago, IL, USA).

2.2. Cell culture

A549, H460, and HEK293T cells were obtained from the American Type Culture Collection (ATCC, Manassas, VA, USA). H596

was obtained from the Cell Bank of the Chinese Academy of Sciences (Beijing, China). A549, A549/shNQO1, H460, H460/shNQO1, H596, and H596/NQO1 cells were cultured in RPMI 1640 (Gibco, Grand Island, NY, USA). HEK293T cells were maintained in Dulbecco's modified Eagle's medium (Gibco). All culture media contain 10% fetal bovine serum (Gibco), 100 U/mL penicillin, and 100 μg/mL streptomycin. Cells were cultured in a 5% CO_2-containing humidified incubator at 37 °C.

2.3. Cell viability assay

Cell viability was evaluated by MTT, LDH release, and ATP levels according to our previous report[28] using the MTT, LDH assay kit, and ATP kit, respectively.

2.4. PI staining

Cells with or without treatment were incubated with PI (5 μg/mL) for 10 min at room temperature in the dark. Images were captured using the Incucyte S3 live cell analysis system (Essen Bioscience, MI, USA).

2.5. Western blotting

Harvested cells and tumor tissues were lysed in RIPA lysis buffer containing PMSF (1 mmol/L) and cocktail (1:50). After protein quantification using BCA protein assay kits (Pierce), a total of 30 μg protein per sample was separated by SDS-PAGE and transferred to polyvinylidene difluoride membranes (Bio-Rad, Richmond, USA). After blocking with 5% nonfat milk for 1 h, the membranes were incubated with primary antibodies (1:1000) overnight at 4 °C, followed by incubation with horseradish peroxidase-conjugated secondary antibodies (1:5000) for 1 h at room temperature. Targeted bands were detected using the ChemiDoc™ Imaging System (Bio-Rad Laboratories, Hercules, CA, USA).

2.6. NQO1 expression and purification

Human *NQO1* genes (GenBank: NP_000894.1) were cloned into pET28a with the N-terminal hexahistidine tag and expressed in BL21 (Beyotime) *Escherichia coli* strain. The bacteria were then grown in kanamycin-resistant LB medium at 37 °C until OD_{600} reached 0.6−0.8. Protein expression was then induced with IPTG (0.5 mmol/L) and cells were further incubated at 18 °C for 16 h. Cells were harvested by centrifugation at 10,000 × *g* (Thermo Scientific, Sorvall LYNX, Waltham, MA, USA) at 4 °C. The cell pellets were resuspended in lysis buffer (10 mmol/L imidazole and 1 mmol/L PMSF in 20 mmol/L Tris-HCl, pH 7.6) and sonicated for 1 h on ice. Soluble proteins were collected from the cell lysate by centrifugation at 15,000 × *g* (Thermo Scientific) for 30 min at 4 °C and then applied to an immobilized Ni-NTA affinity chromatography column (Beyotime) previously equilibrated with binding buffer (BB). After collecting the flow, the column was washed with BB and then eluted with elution buffer (BB containing increasing concentrations of imidazole). The purified protein was concentrated in 10 kD ultrafiltration centrifuge tubes with 20 mmol/L Tris-HCl (pH 7.6). The purity of NQO1 was confirmed by SDS-PAGE with Coomassie blue staining.

2.7. NQO1 activity assay

The enzymatic activity of NQO1 was determined according to our previous report[12]. Briefly, a total reaction system of 200 μL contained 50 μg cell lysates or 50 ng NQO1 protein, 5 μmol/L FAD, 200 μmol/L NADH, and Tris-HCl reaction buffer (25 mmol/L Tris-HCl, pH 7.5, 0.7 mg/mL BSA, 0.01% Tween 20). CTS, β-lap, or DIC was added to the reaction system, and the oxidation reaction of NADH to NAD^+ by NQO1 was monitored at 340 nm for 5 min using a FlexStation 3 microplate reader (Molecular Devices, Sunnyvale, CA, USA).

2.8. Cellular thermal shift assay (CETSA)

CETSA was performed as previously reported[29]. Briefly, A549 or H460 cell lysis was divided into two equal groups with dimethyl sulfoxide or CTS for 0.5 h at room temperature. Then, each group was divided into 7 tubes at the indicated temperatures and heated for 5 min. The heated samples were then centrifuged at 14,000 rpm (Centrifuge 5424R, Eppendorf, Hamburg, Germany) for 20 min at 4 °C, and the supernatant was collected and analyzed by Western blotting.

2.9. Tryptophan fluorescence wavelength assay

Tryptophan fluorescence wavelengths are widely used to monitor changes in proteins and to infer local structure and dynamics[30]. The NQO1 (1 μmol/L) was incubated with CTS at concentrations ranging from 0 to 28 μmol/L for 10 min at room temperature. Protein fluorescence was monitored at excitation and emission wavelengths of 282 nm and 300−380 nm, respectively, using a FluoroMax-4 fully automated spectrofluorometer system (Horiba Jobin Yvon, Bensheim, Germany).

2.10. siRNA silencing

Cells (0.4×10^6) were transfected with siRNAs for 48 h using 5 μL Lipofectamine 3000 (Invitrogen). The siRNA sequences were as follows:

siNQO1-1: 5′-CAGUACACAGAUACCUUGA-3′,
siNQO1-2: 5′-GAACCUCAACUGACAUAUA-3′,
siPARP: 5′-GCAGCUUCAUAACCGAAGATT-3′,
siJNK1: 5′-GCUCAGGAGCUCAAGGAAUTT-3′,
siJNK2: 5′-CCAGCAGCUGAAACCAAUUTT-3′;

Negative control siRNA: 5′-UUCUCCGAACGUGUCACGUTT-3′. All siRNAs were purchased from GenePharma Company (Shanghai, China).

2.11. Measurement of the iron

The iron levels were measured by two different methods: calcein-AM staining and inductively coupled plasma mass spectrometry (ICP-MS). Cells (1.0×10^5) after various treatments were stained with calcein-AM (0.05 μmol/L) for 30 min at 37 °C in the dark. Then, cells were detected by FACScanto™ flow cytometer using the FITC channel (BD Biosciences, San Jose, CA, USA) or the Incucyte S3 live-cell analysis system.

For the ICP-MS, a BCA kit was used to quantify the protein concentration of cells or tissue lysates. A total of 0.5 mL of cell lysate or tumor tissue lysates were thermally digested in 1.5 mL of a 68% HNO_3: H_2O_2 (v/v = 4:1) solution overnight. After digestion, samples were diluted with 2% HNO_3 solution and analyzed by ICP-MS iCAP Q (Thermo Fisher Scientific, Waltham, MA, USA). The iron content of each sample was normalized to the protein concentration and calculated as pg [iron]/mg [protein].

2.12. Laser scanning confocal microscopy

Cells (1.0×10^5) were seeded in the confocal dish for 24 h. Images were captured using a Leica SP8 laser scanning confocal microscope (Leica, Wetzlar, Germany). The fluorescence of calcein-AM, lysosome tracker, and Hochest 33342 was determined at Ex/Em 488/515−560 nm, 577/590 nm, and 361/460−490 nm, respectively.

The immunofluorescence assay was described in a previous study[29]. Briefly, cells (0.5×10^4) were seeded overnight in covered glass-bottom dishes and treated with or without CTS. Cells were fixed with 4% paraformaldehyde in PBS (pH 7.4) for 15 min at room temperature. The fixed cells were then permeabilized with 0.1% Triton X-100 in PBS for 15 min and blocked with PBST blocking buffer (0.1% Tween 20, 1% BSA, and 22.52 mg/mL glycine in PBS) for 1 h at room temperature. Calnexin or NQO1 antibodies (1:100) in blocking buffer were incubated overnight at 4 °C followed by incubation with the second antibody (1:500) for 1 h at room temperature. After Hoechst 33342 staining for 5 min, cells were analyzed using a Leica SP8 laser scanning confocal microscope.

2.13. Construction of NQO1 knockdown cells

The virus was produced by co-transfection of HEK293T cells with pLKO.1-shRNA plasmid, psPAX2, and pMD2.G in a 3:2:1 (*w*/*w*/*w*) ratio, using 4 μL TurboFect (Thermo Scientific) transfection reagent. After 48 and 72 h, the medium containing the secreted virus was harvested and sterile-filtered. The shRNA sequences targeting NQO1 and negative control (Invitrogen) were as follows:

shNQO1-1: 5′-*CCGG* CGAGTCTGTTCTGGCTTATAACTCG AGTTATAAGCCAGAACAGACTCGTTTTTG-3′,

shNQO1-2: 5′-*CCGG* CGAGTGTTCATAGGAGAGTTTCT CGAGAAACTCTCCTATGAACACTCGTTTTTG-3′,

shNQO1-3: 5′-*CCGG* TGGAAGAAACGCCTGGAGAAT CTCGAGATTCTCCAGGCGTTTCTTCCATTTTTG-3′,

Negative control: 5′-*CCGG* GAATCCGCACTACTCCTTACA CTCGAGTGTAAGGAGTAGTGCGGAT TCTTTTTG-3′.

Nucleotides in italics indicate the overhangs introduced into the oligos necessary for cloning into the AgeI site of pLKO.1-TRC.

The target cells were seeded in 6-well plates and incubated with an equal mixture of lentivirus solution and fresh medium for 48−72 h, followed by replacement of the fresh medium with an appropriate concentration of antibiotic until the non-transfected cells were completely dead. The remaining cells were seeded into 96-well plates to obtain single clone cells. After approximately 2 weeks, the single clone cells were expanded and NQO1 expression in each clone was examined by Western blotting.

2.14. Exogenous gene expression

HEK293T cells were transfected with the packaging plasmids psPAX2, and pMD2.G, plus the pLVX vector with NQO1 wild-type or mutant fragments. The construction of stable cell lines was similar to that of the NQO1 knockdown cells. The plasmids of pLVX-NQO1 wild-type and pLVX-NQO1 mutant were purchased from YouBio (Changsha, China).

2.15. Molecular docking

The crystal structure of NQO1 in complex with the inhibitor DIC (PDB 5FUQ, unpublished results) was used as the model for our molecular docking. The chemical structures of tanshinones and β-lap were illustrated using ChemDraw, and the energy was minimized using Chem3D. The resulting structures were then saved as PDB files. The protein and small molecules were prepared with AutoDockTools[31]. AutoDock Vina software was employed to investigate the interaction between the NQO1 protein and small molecules[32]. The docked structures were visualized using Chimera version 1.13.1 and PyMOL (https://pymol.org/edu/)[33]. Ligplot version 2.2.8 was used to generate the 2D diagrams depicting the interaction of tanshinones or β-lap with NQO1[34].

2.16. Measurement of Ca^{2+}

Intracellular and mitochondrial Ca^{2+} levels were determined using fluorescent probes, specifically Fluo-3 AM ester and Rhod-2 AM (Thermo Scientific), respectively. Briefly, cells (1.0×10^5) treated with or without CTS were incubated with Fluo-3 AM (5 μmol/L) or Rhod-2 AM probe (10 μmol/L) at 37 °C for 30 min in the dark. Samples were then analyzed using the FACScanto™ flow cytometer, with the FITC channel for total Ca^{2+} and the PE channel for mitochondrial Ca^{2+} detection.

To further confirm the effect of CTS on Ca^{2+}, cells (0.4×10^6) were transfected with the 2 μg GCaMP3 plasmid (Addgene #22692) using 4 μL Turbofect in 4 mL medium for 48 h. The results were analyzed by a Leica SP8 laser scanning confocal microscope.

2.17. In vivo study

Six-week-old male nude mice weighing between 25 and 30 g were maintained in a laminar flow environment under sterile conditions. Injections of 0.1 mL suspension of H460 cells (4×10^7 cells/mL) or H460 NQO1 knockdown (H460-shNQO1) cells in PBS were administered into the axilla of nude mice. When the average tumor volume reached approximately 50 mm^3, mice injected with H460 cells were randomly divided into the vehicle, CTS (25 mg/kg), and CTS (25 mg/kg) plus DIC (2 mg/kg) co-treatment groups ($n = 7$). Mice injected with H460/shNQO1 were randomly assigned to the vehicle and CTS (25 mg/kg) groups ($n = 7$). CTS and DIC were administered intraperitoneally daily for 15 consecutive days. Tumor volumes and mice body weights were recorded every two days. Tumor volume was measured with a vernier caliper and calculated as Eq. (1):

$$\text{Volume} = \left(\text{Width}^2 \times \text{Length}\right) / 2 \quad (1)$$

When the mice were sacrificed, the tumors were isolated and weighed. All the animal experiments were approved by the Animal Research Ethics Committee of the University of Macau.

2.18. Statistical analysis

Data are expressed as mean ± standard deviation (SD). Statistical analysis was performed using GraphPad Prism 6.0 (GraphPad Software, Inc., La Jolla, CA). Differences between the two groups were compared using a two-sided *t*-test. One-way ANOVA followed by Dunnett's test, or two-way ANOVA followed by the Bonferroni *post hoc* test was used to analyze the differences between more than two groups. *P* values less than 0.05 were considered statistical significance.

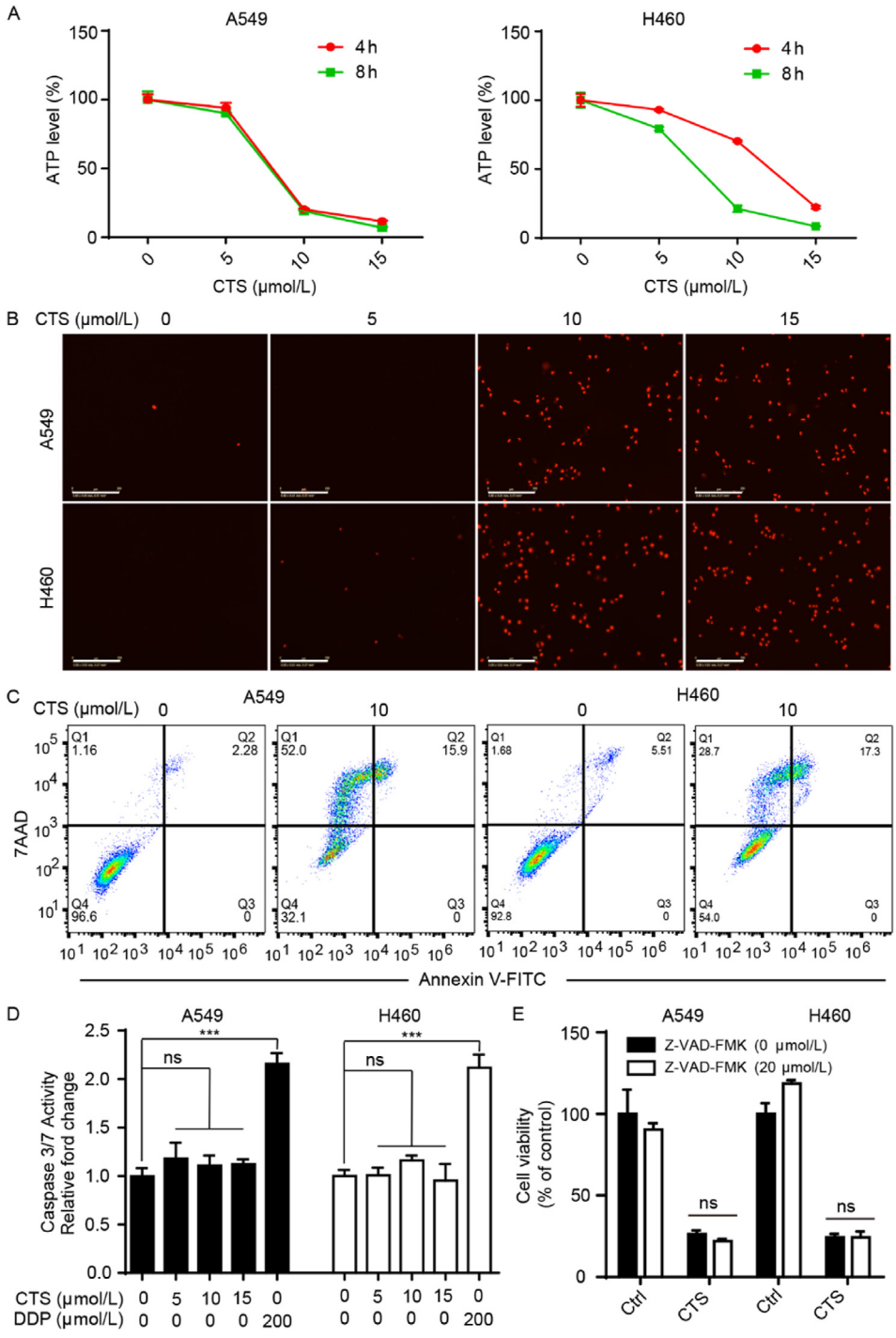

Figure 1 CTS induces non-apoptotic cell death in NSCLC cells. (A) A549 and H460 cells were treated with CTS and the ATP levels were measured using the CellTiter-Glo ATP-based luminescence assay. (B) A549 and H460 cells were treated with CTS for 12 h and then stained with PI. Images were captured using the Incucyte S3 live cell analysis system. Scale bar: 200 μm. (C) Cells were treated with CTS for 12 h and apoptotic cells were detected with Annexin V/7AAD double staining by flow cytometry. (D) Caspase 3/7 activities were determined after CTS or DDP treatment for 6 and 12 h, respectively. DDP (cisplatin) was used as a positive control. (E) Cells were pretreated with Z-VAD-FMK (20 μmol/L) for 1 h, followed by CTS treatment for another 12 h. Cell viability was measured by MTT assay. ns, no significance. ***$P < 0.001$. In (A), (D), and (E), data are presented as mean ± SD, $n = 3$.

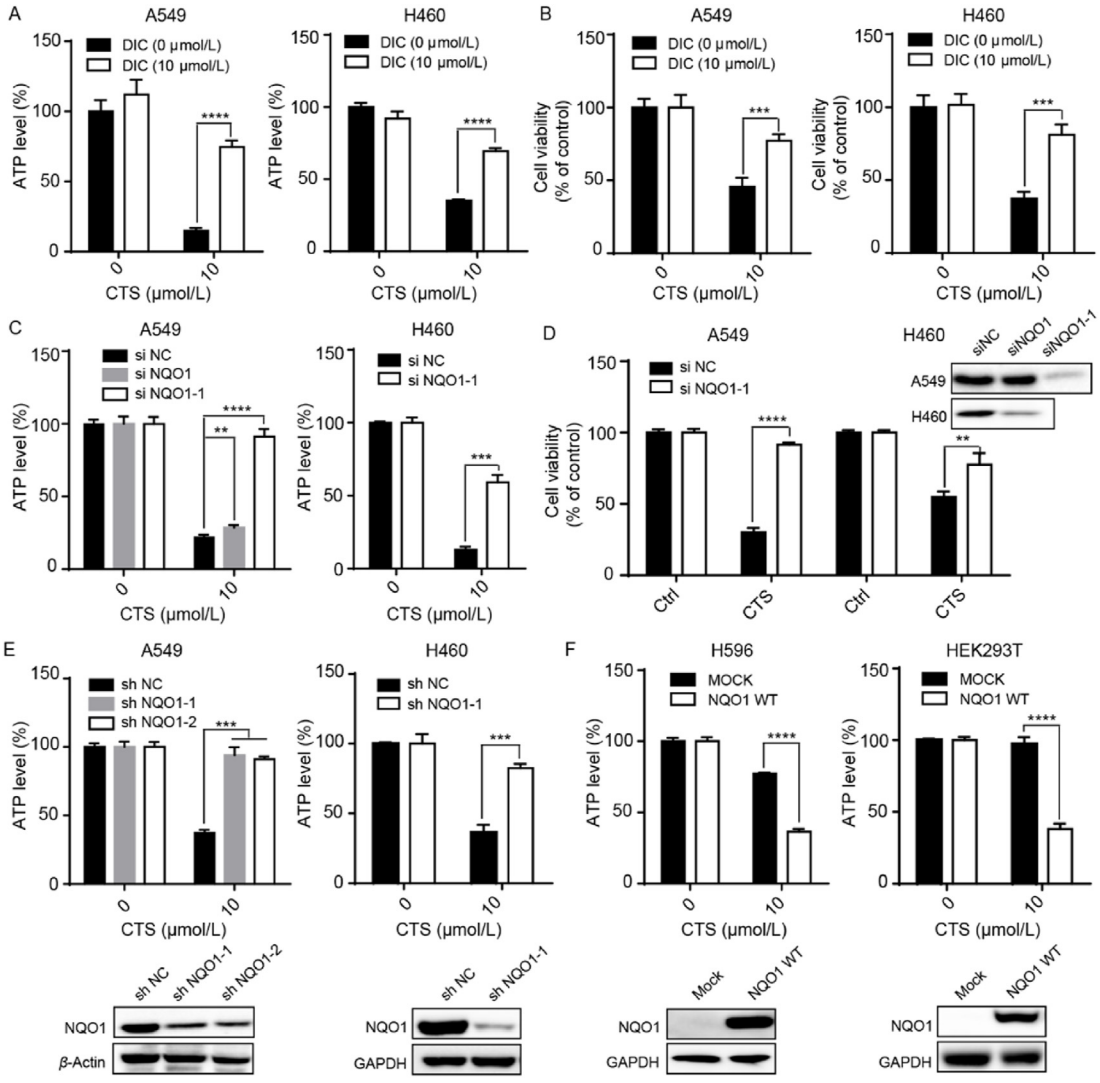

Figure 2 CTS induces NQO1-dependent non-apoptotic cell death. (A, B) ATP levels and cell viability were determined after CTS treatment for 4 and 12 h, respectively, with or without DIC pretreatment for 1 h. (C, D) Cells were transfected with NQO1 siRNA or NC (negative control siRNA) for 48 h and then treated with CTS for 4 and 12 h for the detection of ATP levels (C) and MTT assay (D). (E) NQO1 stable knockdown cells and parental cells were treated with CTS for 4 h and the ATP levels were determined. (F) NQO1 was steadily overexpressed in NQO1$^-$ H596 and HEK293T cells. ATP levels were determined after CTS treatment for 4 h. $^{**}P < 0.01$, $^{***}P < 0.001$, $^{****}P < 0.0001$. Data are presented as mean ± SD, $n = 3$.

3. Results

3.1. *CTS induces non-apoptotic necrosis in NSCLC*

CTS significantly decreased the cell viability of NQO1$^+$ lung cancer cell lines (A549 and H460) in concentration-dependent manners (Supporting Information Fig. S1A). Furthermore, CTS caused a rapid ATP decrease, LDH release, and PI penetration into the cells (Fig. 1A and B, Fig. S1B). Light microscopy and transmission electron microscope (TEM) revealed the appearance of many cytosolic bubbles in the cells (Fig. S1C and S1D). In addition, CTS decreased the spheroid cell viability and 3D spheroid formation in the 3D spheroid assay (Fig. S1E and S1F).

An apoptosis assay was conducted because CTS induces apoptosis in liver, breast, and kidney cancer cells[35,36]. CTS induces a significant increase of 7-AAD(+)/Annexin V(−) cells in both cell lines (Fig. 1C). Furthermore, CTS has no effect on the cleavage of caspases 3/7/8 (Supporting Information Fig. S2A) and the activities of caspases 3/7 (Fig. 1D). In contrast, cisplatin, a chemotherapeutic drug, induces caspase cleavage and increased caspase activities (Fig. 1D and Fig. S2A). The pan-caspase inhibitor Z-VAD-FMK failed to reverse CTS-induced cell death (Fig. 1E). These results indicate that CTS triggers non-apoptotic necrotic cell death.

Biomarkers and specific inhibitors of necroptosis, pyroptosis, paraptosis, and ferroptosis were used to investigate the CTS-induced cell death category. The expression of GSDMD, caspase 1, and GPX4 was not affected by CTS (Fig. S2G and S2H). Furthermore, GSK'827 (receptor-interacting serine/threonine kinase 3 inhibitor), NSA (mixed lineage kinase domain-like inhibitor), glycine (cytoprotective effects in pyroptosis), VX765 (caspase 1 inhibitor), CHX (paraptosis inhibitor), IM54 (necrosis inhibitor), and Fer-1 (ferroptosis inhibitor) were unable to reverse CTS-induced cell death (Fig. S2B−S2F).

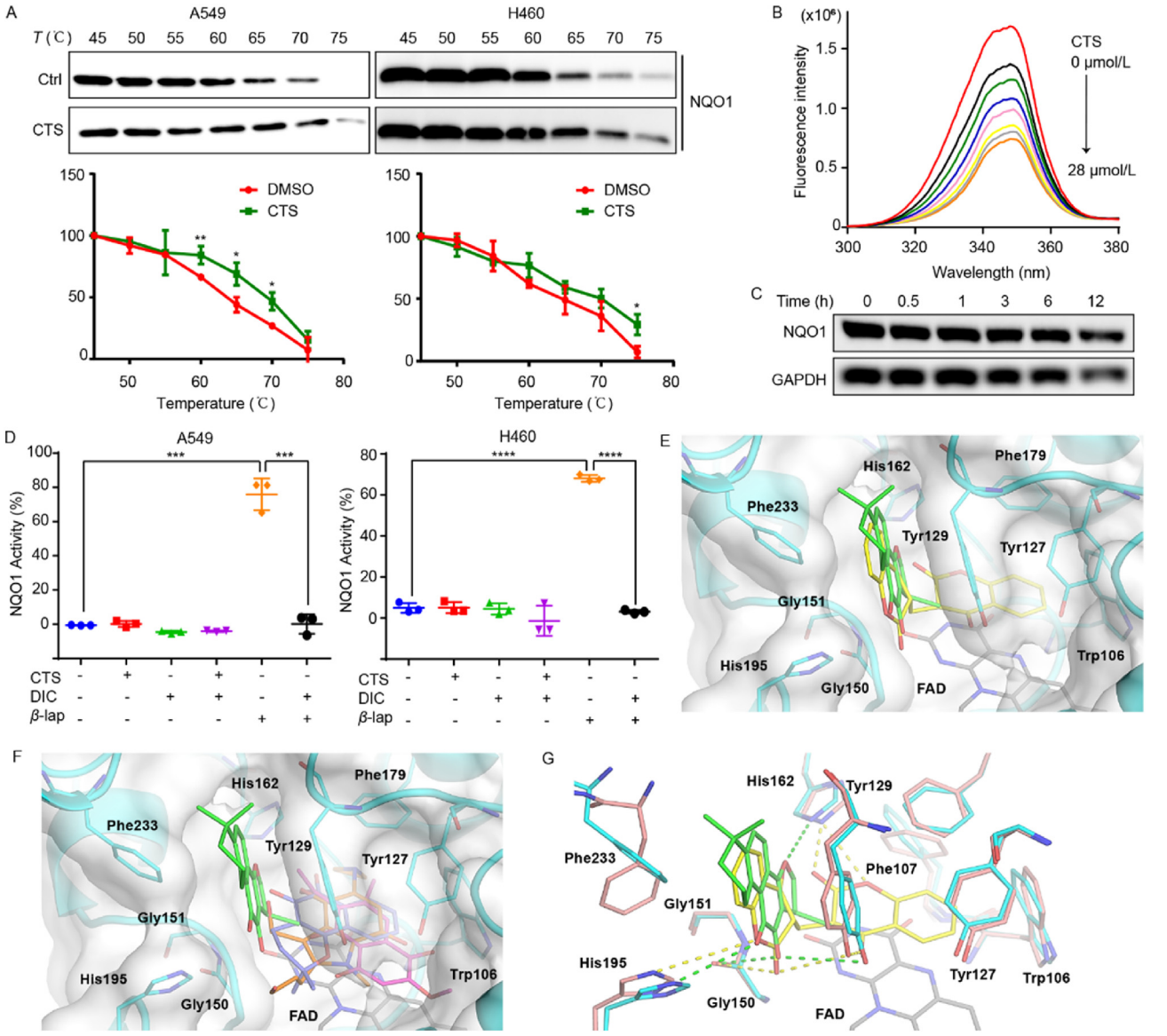

Figure 3 CTS targets the non-enzymatic function of NQO1. (A) CETSA determined the binding between CTS and NQO1. Cell lysates with or without CTS were heated at the indicated temperature. NQO1 levels were calculated by Western blotting and quantitative analysis. (B) Fluorescence titration was used to determine the interaction between CTS and NQO1. Recombinant NQO1 (1 μmol/L) was titrated with CTS (0, 4, 8, 12, 16, 20, 24, and 28 μmol/L). (C) A549 cells were treated with CTS (10 μmol/L) and the NQO1 levels were determined by Western blotting. (D) A549 and H460 cell lysates were exposed to CTS with or without DIC and the NQO1 activities were determined. β-Lap was used as a positive control. (E) Overview of the catalytic site of the NQO1-CTS docked structure superposed to the NQO1 structure in complex with DIC (PDB 5FUQ). (F) Overview of the catalytic site of the NQO1-CTS docked structure superimposed to the NQO1 structure in complex with the compounds β-lap (violet sticks), the chemotherapeutic drug E09 (PDB 1GG5) (orange sticks), and the MAM (pink sticks). All protein residues at the catalytic site are shown as sticks. (G) Hydrogen bond interactions with residues at the catalytic site as determined by CTS (green sticks) and DIC (yellow sticks). All protein residues at the catalytic site are shown as sticks in cyan for the NQO1-CTS docked structure and in salmon for the NQO1-DIC structure (PDB 5FUQ). *$P < 0.05$, **$P < 0.01$, ***$P < 0.001$, ****$P < 0.0001$. In (A) and (D), data are presented as mean ± SD, $n = 3$.

3.2. *CTS-induced necrosis is NQO1-dependent*

CTS-induced cell death is significantly reversed by DIC, a potent and competitive inhibitor of NQO1 (Fig. 2A and B). Transient silencing and stable knockdown of NQO1 show similar effects (Fig. 2C–E). CTS has no cytotoxic effect on the NQO1 negative ($NQO1^-$) cell lines H596 and HEK293T. In contrast, NQO1 transfection significantly sensitizes the effect of CTS (Fig. 2F). Notably, the significant cytotoxic effect of CTS is observed only in $NQO1^+$ and not in $NQO1^-$ cells (Supporting Information Fig. S3A and S3B). This suggests that CTS selectively killed $NQO1^+$ cancer cells.

3.3. *Non-enzymatic function of NQO1 contributes to CTS-induced necrosis*

CTS significantly increased NQO1 stability in both A549 and H460 cells in the CETSA assay, indicating the direct binding of CTS to NQO1 (Fig. 3A). The interaction between CTS and NQO1 is confirmed by the fluorescence quenching assay (Fig. 3B). While CTS upregulates *NQO1* mRNA levels, it does not affect the translocation and protein expression of NQO1 (Fig. 3C and Supporting Information Fig. S4A and S4B). In particular, CTS shows no effect on NQO1 catalytic activity in enzymatic activity assays using A549 and H460 cell lysates (Fig. 3D) and recombinant NQO1 protein (Fig. S4C). In contrast, β-lap, an NBD, significantly increased NQO1 activities, which was inhibited by DIC (Fig. 3D and Fig. S4C).

To gain further insight into the molecular determinants of the interaction of CTS with NQO1, we performed molecular docking using the X-ray structure of NQO1 in complex with the inhibitor DIC (PDB 5FUQ, unpublished results), as a reference model and compared it with other previously reported NQO1 structures. The docked structure of NOQ1 with CTS, shows that CTS is positioned between Tyr129 and Phe 233 in an orientation similar to that reported in the X-ray structure of NQO1 in complex with DIC (PDB 5FUQ) (Fig. 3E). Then, we further compared the docked structures of substrates with CTS, including β-lap, the chemotherapeutic drug E09 (PDB 1GG5)[37] and MAM (docking structure previously reported by our group)[12] (Fig. 3F). Results show that CTS positions a different binding site in NQO1 compared to other substrates/inhibitors that interact with NQO1 through the isoalloxazine ring by positioning in a parallel orientation to the FAD. Furthermore, our docking results show that the binding mode of CTS is also quite similar to that observed for DIC, forming hydrogen bond interactions with the enzyme at Phe 107, Tyr129, Gly 150, and His 195 (Fig. 3G). In addition, the mutant of sites Tyr129 and Gly150 in H596 cells impaired the cytotoxity of CTS (Fig. S4D). Thus, these results indicate that CTS does not bind to NQO1 at the canonical catalytic site but near it. This may be the main reason why CTS does not affect NQO1 activity.

CTS belongs to a family of natural cytotoxic compounds called tanshinones. They share a similar orthoquinone structure (Supporting Information Fig. S5A). However, tanshinones exhibit different effects on NQO1 activities (Fig. S5G). Although dihydrotanshinone I and tanshinol A moderately increase NQO1 activities, their cytotoxic effects cannot be reversed by DIC (Fig. S5B, S5C and S5G). TSB, tanshinone IIB (TanIIB), and tanshinone IIA exhibit different effects on NQO1 activities, but their cytotoxicities are all significantly reversed by DIC (Fig. S5D−S5G). The docking results reveal that TSB, TanIIB, and tanshinone IIA can enter the binding pocket of NQO1, of which TSB and TanIIB can form hydrogen bonds with NQO1 (Fig. S5H).

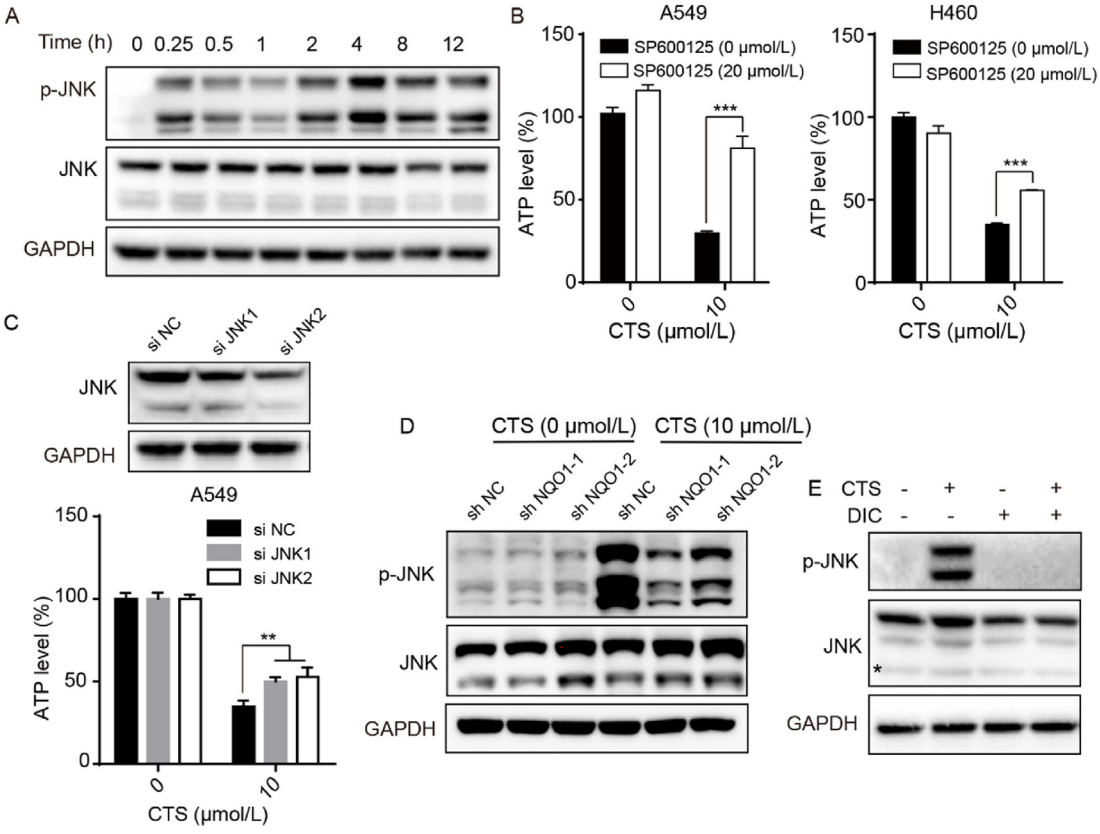

Figure 4 CTS triggers sustained JNK1/2 activation. (A) Effect of CTS on JNK1/2 expression and phosphorylation in A549 cells. (B) Cells were treated with CTS for 4 h with or without SP600125 pretreatment for 1 h and the ATP levels were determined. (C) Cells were transfected with JNK1/2 siRNAs for 48 h and then treated with CTS for 4 h. The ATP levels were measured. (D) NQO1 knockdown cells were treated with CTS for 0.5 h and the activation of JNK1/2 was detected. (E) Cells were treated with CTS for 0.5 h with or without DIC pretreatment for 1 h. The activation of JNK1/2 was detected. $^{**}P < 0.01$, $^{***}P < 0.001$. In (B) and (C), data are presented as mean ± SD, $n = 3$.

3.4. JNK 1/2 activation involved in CTS-induced necrosis

JNK1/2 activation actively contributes to β-lap-induced cell death in NQO1 overexpressing MDA-MB-231 cells[38] and embryonic fibroblasts[39]. CTS induces sustained JNK1/2 phosphorylation (Fig. 4A). Furthermore, JNK1/2 inhibitor SP600125 pretreatment or JNK1/2 knockdown can significantly reverse CTS-induced ATP decrease (Fig. 4B and C). In addition, DIC or NQO1 knockdown dramatically decreased JNK1/2 phosphorylation (Fig. 4D and E). Thus, these results suggest that JNK1/2 plays a crucial role in NQO1-dependent necrosis induced by CTS.

3.5. NQO1-mediated iron release contributes to CTS-induced necrosis

CTS induces a significant quenching of calcein-AM fluorescence, suggesting an increase in intracellular iron levels (Fig. 5A and B). The CTS-induced increase in cellular iron is further detected by ICP-MS (Fig. 5C). The combination of lysotracker localization and calcein-AM staining reveals an increase of iron in lysosomes after CTS treatment (Fig. 5D). Furthermore, the iron chelators DFO and DFP significantly reversed CTS cytotoxicity (Fig. 5E and F) whereas the iron donors $FeSO_4$ and ferric ammonium

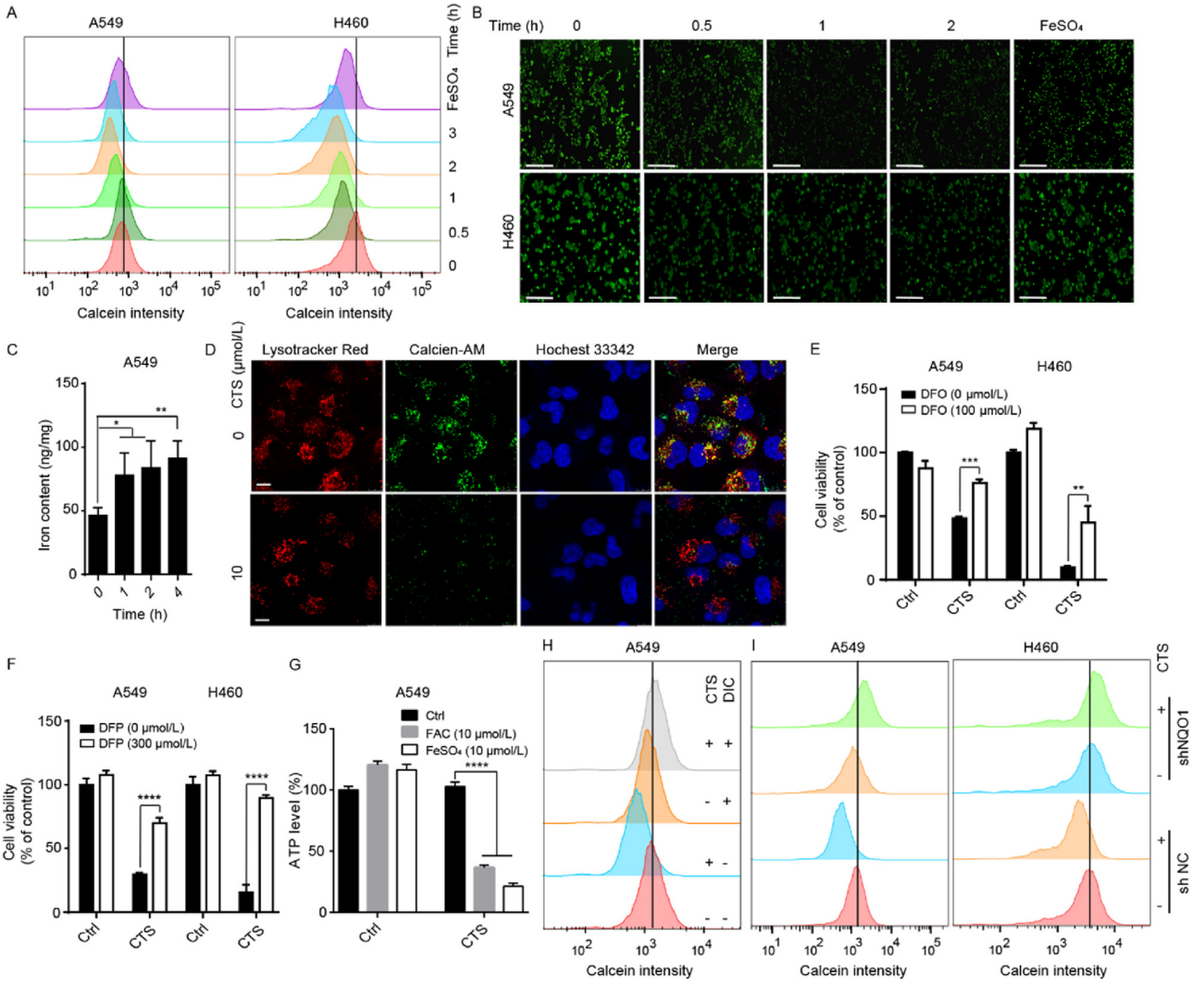

Figure 5 Involvement of iron in CTS-induced cell death. Cells treated with CTS (10 μmol/L) were stained with calcein-AM and then analyzed by flow cytometry (A) or the Incucyte S3 live-cell imaging system (B). Scale bar: 200 μm. Iron levels in whole A549 cell lysates were determined by ICP-MS (C), data are presented as mean ± SD, $n = 3-4$. A549 cells were loaded with calcein-AM (1 μmol/L) for 1 h at 4 °C and then treated with CTS for 3 h followed by staining with lysotracker red and Hochest 33342. Images were captured with a confocal system (D). Scale bar: 10 μm. A549 cells were pretreated with DFO, DFP, ferric ammonium citrate, and $FeSO_4$ for 1 h and then treated with CTS for another 12 h (E, F) or 1 h (G). MTT assay (E, F) and ATP levels (G) were analyzed. Cells were exposed to CTS for 3 h with or without DIC pretreatment for 1 h. Iron accumulation was detected by calcein-AM using flow cytometry (H). Wild type and NQO1 knockdown cells were treated with CTS for 3 h. Iron accumulation was detected by calcein-AM using flow cytometry (I). $^*P < 0.05$, $^{**}P < 0.01$, $^{***}P < 0.001$, $^{****}P < 0.0001$. In (E), (F), and (G), data are presented as mean ± SD, $n = 3$.

citrate enhanced it (Fig. 5G). Nevertheless, Fer-1 fails to reverse CTS-induced necrosis and CTS has no effect on GPX4 expression (Fig. S2D and S2H). In contrast, DIC significantly inhibits CTS-induced increase in iron (Fig. 5H), and a similar reversal effect is observed with NQO1 silencing (Fig. 5I). Iron promotes lipid peroxidation causing oxidative damage to organelles[40]. CTS

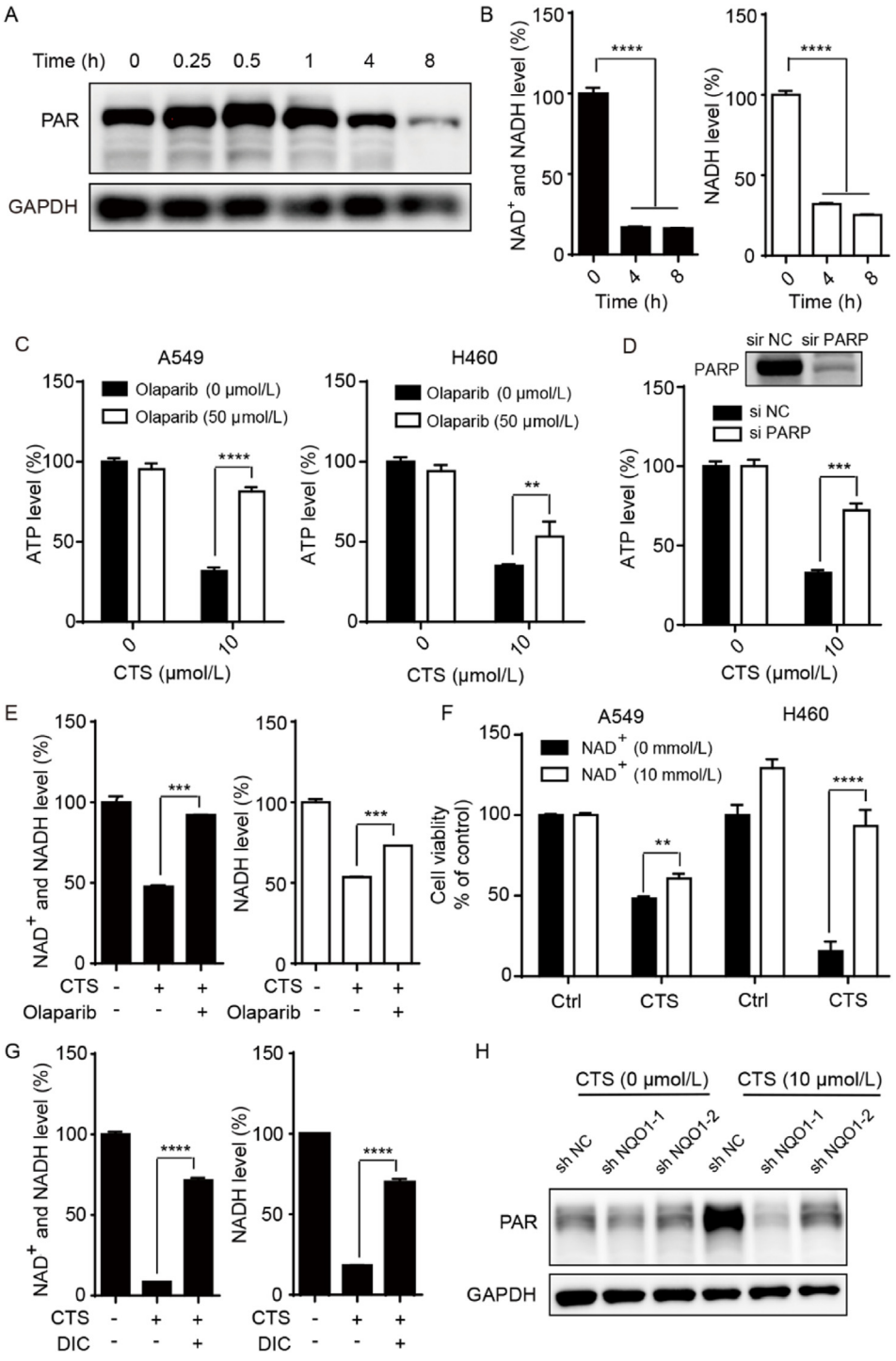

Figure 6 NAD^+ depletion contributes to CTS-induced cell death. A549 cells were treated with CTS and PAR expression was detected (A). A549 cells were treated with CTS and the total NAD^++NADH and NADH levels were determined (B). A549 cells were treated with CTS for 4 h (C) or 12 h (F) with or without olaparib (C) or NAD^+ (F) pretreatment for 1 h. ATP levels (C) or MTT assay (F) were performed. A549 cells with PARP silencing were treated with CTS for 4 h. ATP levels were determined (D). A549 cells were treated with CTS for 2 h with or without olaparib or DIC pretreatment for 1 h. The levels of total NAD^++NADH and NADH were determined (E, G). A549 cells or NQO1 knockdown A549 cells were treated with CTS for 1 h, and the PAR expression was determined (H). $^{**}P < 0.01$, $^{***}P < 0.001$, $^{****}P < 0.0001$. Data are presented as mean ± SD, $n = 3$.

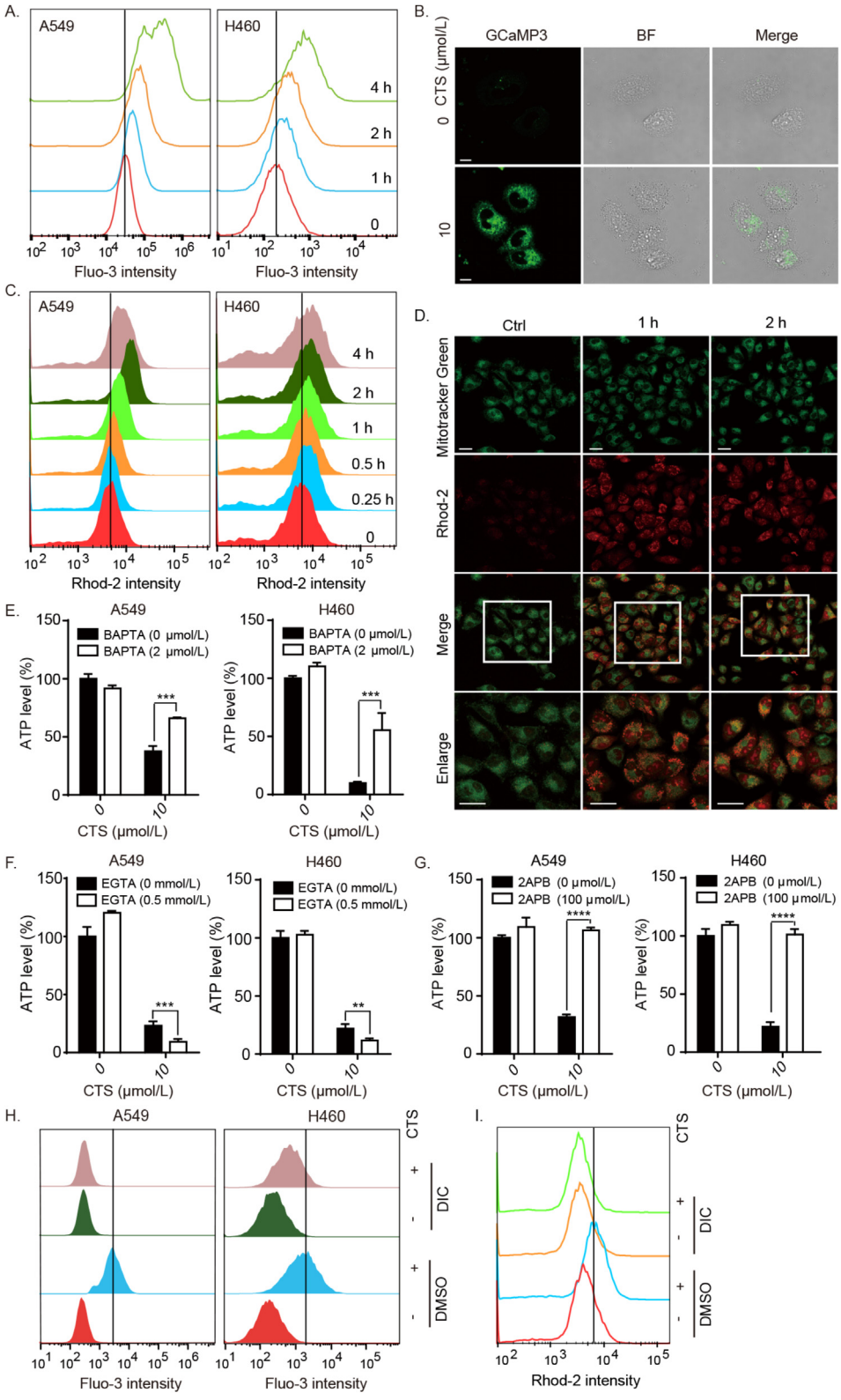

Figure 7 Cytosolic and mitochondrial Ca^{2+} overload triggers CTS-induced necrosis. Cells were treated with CTS (10 μmol/L) followed by the Fluo-3 AM staining and flow cytometry (A). A549 cells were transfected with GCaMP3 plasmid for 48 h and then treated with CTS for 2 h. Images were captured with a confocal system; Scale bar: 10 μm (B). Cells were treated with CTS and the Ca^{2+} levels were stained with Rhod-2 AM and detected by flow cytometry (C) and a confocal imaging system; Scale bar: 25 μm (D). Cells were exposed to CTS with or without pretreatment with BAPTA (E), EGTA (F), and 2APB (G) for 1 h and the ATP levels were measured. Cells were treated with CTS for 4 h with or without DIC (10 μmol/L) and then stained with Fluo-3 AM (H) or Rhod-2 AM (I) followed by flow cytometry. $^{**}P < 0.01$, $^{***}P < 0.001$, $^{****}P < 0.0001$. In (E), (F), and (G), data are presented as mean ± SD, $n = 3$.

induces lipid peroxidation and damage to the endoplasmic reticulum (ER) and mitochondria (Fig. S1D and Supporting Information Fig. S6), which may also contribute to CTS-induced necrosis.

3.6. NAD^+ depletion contributes to CTS-induced necrosis

PARP activation and NAD^+ depletion mediate NQO1-induced cell death in response to β-lap[14,16]. Although CTS shows no effect on NQO1 activation, it increases PAR and decreases total NAD^+ and NADH (Fig. 6A and B). Furthermore, both the PARP inhibitor olaparib and PARP silencing can significantly reverse CTS-induced PAR accumulation, NAD^+ depletion, and cell death (Figs. 6C–E, 8D). NAD^+ supplementation effectively reverses CTS-induced cell death (Fig. 6F). Meanwhile, both NQO1 shRNA and DIC significantly reverse CTS-induced PAR accumulation and NAD^+ depletion (Fig. 6G and H). Thus, CTS-induced necrosis involves NQO1-mediated PARP activation and NAD^+ depletion.

3.7. Cytosolic and mitochondrial Ca^{2+} overload triggers CTS-induced necrosis

Ca^{2+} is an upstream modulator of PARP-1 activation and DNA repair in mediating β-lap-induced cell death[41]. CTS increases cytoplasmic Ca^{2+} levels in a time-dependent manner (Fig. 7A). A Ca^{2+} indicator plasmid shows a similar result (Fig. 7B). The

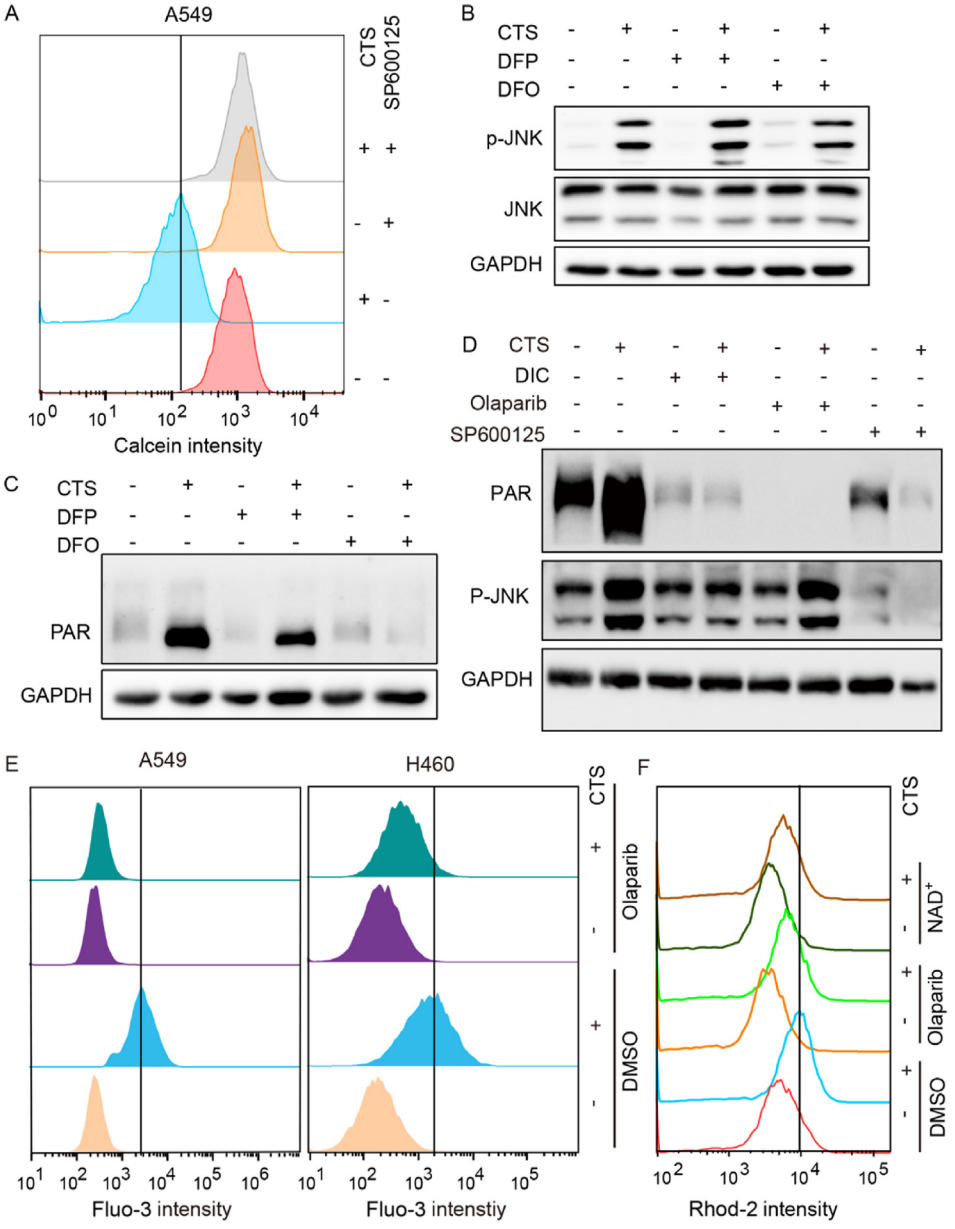

Figure 8 CTS induces an NQO1/JNK/iron/PARP/calcium-dependent necrosis. Cells were exposed to CTS for 3 h with or without SP600125 pretreatment for 1 h, and iron levels were stained with calcein-AM (A). A549 cells were pretreated with DFO (100 μmol/L), DFP (300 μmol/L), DIC (10 μmol/L), olaparib (50 μmol/L), or SP600125 (20 μmol/L) for 1 h, followed by CTS for 0.5 h. The expression of JNK1/2, phosphor-JNK1/2, and PAR were determined (B–D). Cells treated with CTS with or without olaparib (50 μmol/L), and NAD^+ (10 mmol/L) were stained with Fluo-3 AM (E) or Rhod-2 AM (F).

mitochondrial Ca^{2+} level is also significantly increased after CTS treatment (Fig. 7C and D). BAPTA, an intracellular Ca^{2+} chelating agent, significantly reverses CTS-induced cell death whereas EGTA, an extracellular Ca^{2+} chelator, fails to do so (Fig. 7E and F). 2APB, a Ca^{2+} channel inhibitor, significantly reverses CTS-triggered cytosolic and mitochondrial Ca^{2+} levels and cell death (Fig. 7G, Supporting Information Fig. S7). In addition, DIC significantly reverses CTS-triggered cytosolic and mitochondrial Ca^{2+} levels (Fig. 7H and I). Thus, cytosolic and mitochondrial Ca^{2+} are important mediators of CTS-induced cell death.

3.8. *CTS induces an NQO1/JNK1/2/Iron/PARP/Ca^{2+}-dependent necrosis*

SP600125 significantly reduces CTS-induced iron increase and PAR activation (Fig. 8A and D). Although DFO and DFP show no effect on CTS-induced JNK1/2 activation (Fig. 8B), they significantly prevent PAR over-consumption (Fig. 8C). Olaparib or NAD^+ pretreatment significantly reverses the cytosolic and mitochondrial Ca^{2+} accumulation (Fig. 8E and F). In contrast to DIC and SP600125, olaparib fails to inhibit JNK1/2 activation (Fig. 8D). These observations reveal that NQO1 is upstream in regulating JNK1/2 activation, iron release, NAD^+ depletion, and Ca^{2+} accumulation in response to CTS.

3.9. *CTS inhibits NQO1-dependent tumor growth*

CTS significantly inhibits the tumor volume and weight in the H460 xenograft nude mouse model. However, this effect is abolished by DIC co-administration (Fig. 9A–C). CTS shows no anticancer effect on the H460/shNQO1 xenograft nude mice model (Fig. 9D–F). Furthermore, CTS significantly increases the iron content in tumor tissues, which is reversed by DIC co-administration and NQO1 silencing (Fig. 9G and H). The activation of PAR and JNK1/2 is observed in CTS-treated tumor tissues, which is also inhibited by DIC co-treatment (Fig. 9I). In addition, CTS shows no anticancer effect in xenograft zebrafish model derived from $NQO1^-$ cell line H596 (Supporting Information Fig. S8A and S8B). In contrast, both DIC and DFP nearly

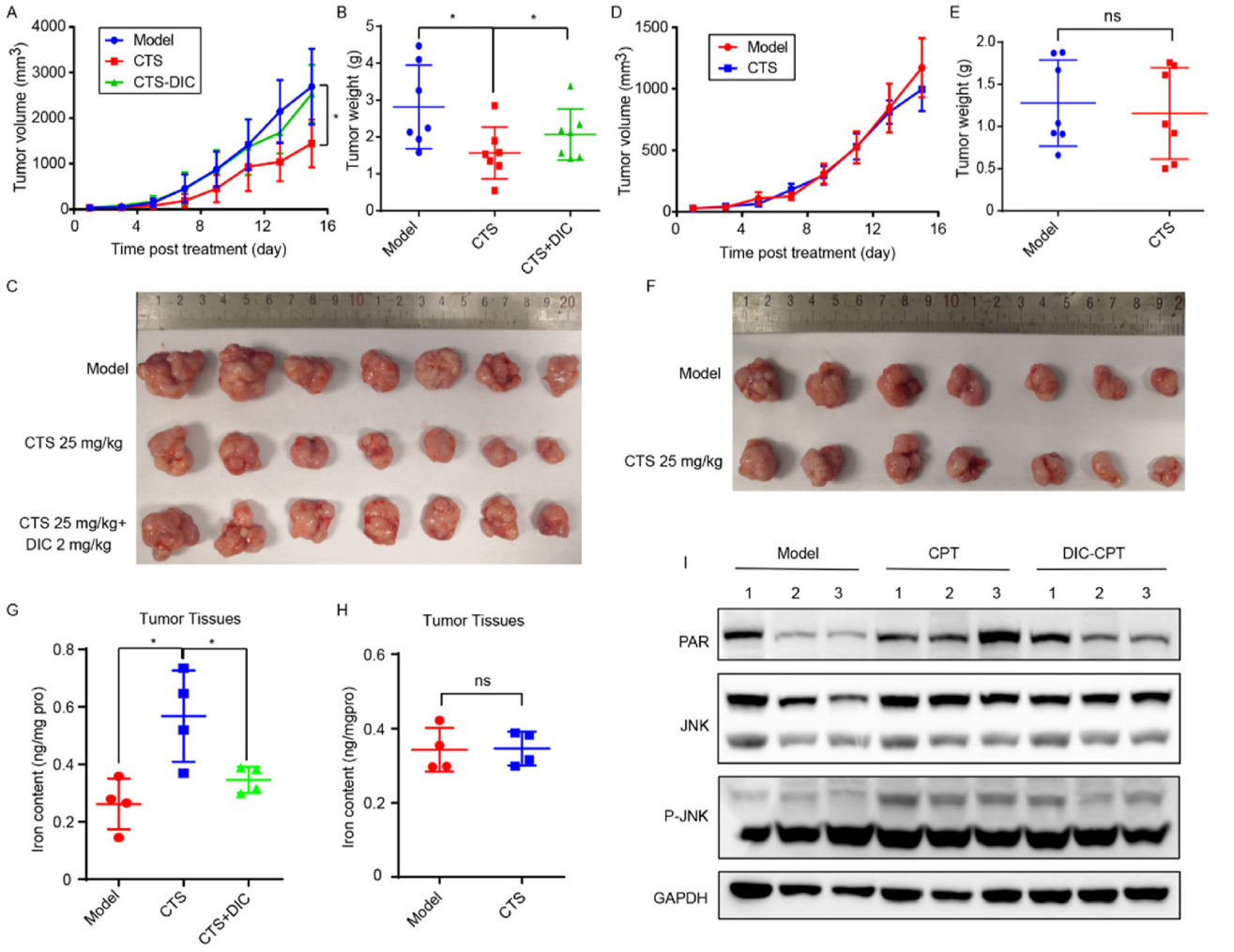

Figure 9 CTS inhibits tumor growth in the nude mouse xenograft model. Effect of CTS (25 mg/kg) on tumor volume and weight after 15 days treatment with or without DIC (2 mg/kg) co-treatment in H460-derived nude mice (A–C). Effect of CTS (25 mg/kg) on tumor volume and weight after 15 days treatment in H460/shNQO1-derived nude mice (D–F), data are presented as mean ± SD, $n = 7$. Iron levels in tumor tissues from H460 (G) and H460/shNQO1 (H) derived nude mice were detected by ICP-MS, data are presented as mean ± SD, $n = 4$. (I) Protein expression of JNK1/2, phosphor-JNK1/2, and PAR in tumor tissues. $^*P < 0.05$, ns, no significance.

completely reverse the anticancer effect of CTS in the xenograft zebrafish model derived from NQO1$^+$ cell line A549 (Fig. S8C and S8D).

4. Discussion

The anticancer effect of NBDs has been widely investigated[12,14,42,43]. Here, we report a non-enzymatic dependent necrosis mediated by NQO1. Key findings of this study include: (1) CTS selectively induces an NQO1-dependent non-apoptotic necrosis in NQO1$^+$ cancer cells. (2) CTS-induced necrosis is dependent on the non-enzymatic function of NQO1 and is facilitated by the JNK1/2−iron−PARP−Ca^{2+} pathway. (3) CTS inhibits tumor growth *in vivo* in an NQO1-dependent manner.

Consistent with previous reports[27,44], CTS induces cell death in lung cancer cells, a finding verified by the 3D tumor sphere model. CTS kills cancer cells by apoptosis induction mediated by ROS, STAT3, and caspase 3, among others[45-47]. However, Annexin V/7AAD double staining does not provide evidence of apoptosis after CTS treatment. CTS does not affect the cleavage and activity of caspase 3/7 and the pan-caspase inhibitor is ineffective at reversing CTS-induced cell death. Furthermore, classic apoptotic features are not observed in TEM. In contrast, necrotic cell death features such as LDH release, PI penetration, and ATP depletion[48,49] are all observed after CTS treatment. Thus, CTS induces non-apoptotic necrosis in NSCLC.

Programmed necrosis such as necroptosis, paraptosis, pyroptosis, and ferroptosis is precisely controlled by key regulators such as receptor-interacting serine/threonine kinase 3, mixed lineage kinase domain-like, caspase 1, GSDMD, GPX4 and can be significantly reversed by specific inhibitors such as GSK'872, NSA, VX765, CHX, Fer-1, etc.[50,51]. However, CTS does not affect these key regulators and the specific inhibitors fail to reverse CTS-induced necrosis. Thus, CTS-induced necrosis does not fit into any of the programmed necrosis categories. Our previous report shows that DIC inhibits CTS-induced cell death in A549 cells[27]. Here, we dissected the critical role of NQO1 in mediating CTS-induced necrosis. CTS selectively kills NQO1$^+$ cancer cells, which can be significantly reversed by DIC and NQO1 silencing. Transfection of NQO1 to NQO1$^-$ cells dramatically increases their sensitivity to CTS. Thus, NQO1 appears to be the direct target of CTS that causes its cytotoxic effect in NQO1$^+$ cancer cells.

NBDs, such as β-lap, target NQO1 by increasing NQO1 enzymatic activities[52]. In contrast to β-lap, CTS shows no effect on NQO1 activity. Moreover, the docking structures show that CTS is positioned in a narrow cavity between Tyr129 and Phe 233, two highly flexible residues[53,54] and key players in the enzymatic function of NQO1. CTS is located in the side active pocket which is quite similar to that observed for DIC. However, it does not have a parallel interaction with FAD. β-Lap/MAM parallel with the isoalloxazine ring of FAD to form a stable $\pi-\pi$ interaction which is a stable and favorable pose for the electron transport between NQO1 and substrates[8]. Three mutations in the binding sites of NQO1 can partially reverse CTS-induced necrosis suggesting that these mutations cannot maintain the favorable structure for CTS binding. However, further investigation is needed to determine the detailed mechanism.

The effect of CTS on NQO1 is distinctive compared to other tanshinones, which show substantial variation in NQO1 activity. Our previous study shows that TSB binds and activates NQO1, leading to NQO1-dependent necrosis[15]. Unlike CTS, TSB has a parallel structure to FAD and forms hydrogen bonds with NQO1 in molecular docking. Therefore, slight variations in the chemical structure could influence the binding pattern and activity of tanshinones on NQO1, making it a fascinating subject to study.

ROS generation, JNK1/2 activation, PARP hyperactivation, Ca^{2+} elevation, PAR accumulation, ATP, and NAD^+ depletion following NQO1 activation are well documented in response to β-lap[14,17,52,55]. The inhibitory effects of SP600125, DFO, DFP, olaparib, BAPTA-AM, NAD^+, siRNA for JNK1/2 and PARP, etc., confirm the involvement of JNK1/2, iron, PARP, and Ca^{2+} in CTS-induced necrosis. Consistent with our previous report[27], CTS induces ROS generation (data not shown). Surprisingly, the ROS does not originate from NQO1, as neither DIC nor NQO1 silencing reversed ROS generation (data not shown). This is a contrasting observation because β-lap-induced ROS is NQO1-dependent[14,55]. Further research is needed to investigate the sources of ROS in response to CTS. NQO1 activation by MAM results in iron elevation, which contributes to NQO1-dependent necrosis[42]. CTS induces iron elevation and necrosis, which are significantly reversed by NQO1 silencing or DIC. Thus, iron is essential for CTS-induced necrosis. Together with increased lipid peroxidation, CTS-induced cell death may be closely related to ferroptosis[56]. The combination of β-lap and olaparib shows a synergistic anticancer effect in NQO1$^+$ tumors[57]. However, olaparib undermines the anticancer effect of CTS, providing further evidence of the difference between CTS and β-lap on NQO1.

The critical role of NQO1 in CTS-induced anticancer effect was further confirmed *in vivo* using both zebrafish and nude mouse models. CTS significantly inhibited tumor growth in xenograft models derived from NQO1$^+$ cells, which was reversed by co-treatment with DIC, NQO1 silencing, or DFP. Furthermore, consistent with the cellular results, iron accumulation and activation of JNK1/2 and PAR were also observed in tumor tissues and these effects were inhibited by co-treatment with DIC or NQO1 silencing.

5. Conclusions

In conclusion, CTS induces NQO1-dependent non-apoptotic necrosis, which is mediated by the activation of JNK1/2 and PARP, the accumulation of iron and Ca^{2+}. In contrast to NBDs, CTS does not activate NQO1 enzymatic activities. This study uncovers a potential molecular target for CTS and presents a novel NQO1-based strategy for anticancer drug development that exploits the non-enzymatic function of NQO1.

Acknowledgments

This work was supported by the Science and Technology Development Fund, Macao S.A.R (FDCT) (0070/2022/A2, 005/2023/SKL, China), the National Natural Science Foundation of China (82173848), the Research Fund of University of Macau (MYRG2020-00053-ICMS, MYRG-GRG2023-00072-ICMS-UMDF, China), and the Ministry of Education Frontiers Science Centre for Precision Oncology, University of Macau (SP2023-00001-FSCPO, China).

Author contributions

Ying Hou: Writing − original draft, Project administration, Methodology, Data curation, Conceptualization. Bingling Zhong:

Methodology, Data curation. Lin Zhao: Methodology, Data curation. Heng Wang: Methodology, Data curation. Yanyan Zhu: Methodology, Data curation. Xianzhe Wang: Methodology, Data curation. Haoyi Zheng: Visualization, Software. Jie Yu: Methodology. Guokai Liu: Methodology. Xin Wang: Writing − review & editing. Jose M. Martin-Garcia: Methodology. Xiuping Chen:Writing − review & editing, Supervision, Funding acquisition, Conceptualization.

Conflicts of interest

The authors declare no potential conflicts of interest.

Appendix A. Supporting information

Supporting information to this article can be found online at https://doi.org/10.1016/j.apsb.2024.12.005.

References

1. Leiter A, Veluswamy RR, Wisnivesky JP. The global burden of lung cancer: current status and future trends. *Nat Rev Clin Oncol* 2023;**20**:624−39.
2. Zappa C, Mousa SA. Non-small cell lung cancer: current treatment and future advances. *Transl Lung Cancer Res* 2016;**5**:288−300.
3. Karuppasamy R, Veerappapillai S, Maiti S, Shin WH, Kihara D. Current progress and future perspectives of polypharmacology: from the view of non-small cell lung cancer. *Semin Cancer Biol* 2021;**68**:84−91.
4. Cadenas E. Antioxidant and prooxidant functions of DT-diaphorase in quinone metabolism. *Biochem Pharmacol* 1995;**49**:127−40.
5. Jin Q, Wu J, Wu Y, Li H, Finel M, Wang D, et al. Optical substrates for drug-metabolizing enzymes: recent advances and future perspectives. *Acta Pharm Sin B* 2022;**12**:1068−99.
6. Oh ET, Park HJ. Implications of NQO1 in cancer therapy. *BMB Rep* 2015;**48**:609−17.
7. Beaver SK, Mesa-Torres N, Pey AL, Timson DJ. NQO1: a target for the treatment of cancer and neurological diseases, and a model to understand loss of function disease mechanisms. *Biochim Biophys Acta Proteins Proteom* 2019;**1867**:663−76.
8. Zhang K, Chen D, Ma K, Wu X, Hao H, Jiang S. NAD(P)H:quinone oxidoreductase 1 (NQO1) as a therapeutic and diagnostic target in cancer. *J Med Chem* 2018;**61**:6983−7003.
9. Belinsky M, Jaiswal AK. NAD(P)H:quinone oxidoreductase 1 (DT-diaphorase) expression in normal and tumor tissues. *Cancer Metastasis Rev* 1993;**12**:103−17.
10. Gerber DE, Beg MS, Fattah F, Frankel AE, Fatunde O, Arriaga Y, et al. Phase 1 study of ARQ 761, a β-lapachone analogue that promotes NQO1-mediated programmed cancer cell necrosis. *Br J Cancer* 2018;**119**:928−36.
11. Ross D, Siegel D. The diverse functionality of NQO1 and its roles in redox control. *Redox Biol* 2021;**41**:101950.
12. Yu J, Zhong B, Jin L, Hou Y, Ai N, Ge W, et al. 2-Methoxy-6-acetyl-7-methyljuglone (MAM) induced programmed necrosis in glioblastoma by targeting NAD(P)H:quinone oxidoreductase 1 (NQO1). *Free Radic Biol Med* 2020;**152**:336−47.
13. Froeling FE, Swamynathan MM, Deschênes A, Chio IIC, Brosnan E, Yao MA, et al. Bioactivation of napabucasin triggers reactive oxygen species-mediated cancer cell death. *Clin Cancer Res* 2019;**25**:7162−74.
14. Huang X, Dong Y, Bey EA, Kilgore JA, Bair JS, Li LS, et al. An NQO1 substrate with potent antitumor activity that selectively kills by PARP1-induced programmed necrosis. *Cancer Res* 2012;**72**:3038−47.
15. Zhong B, Yu J, Hou Y, Ai N, Ge W, Lu JJ, et al. A novel strategy for glioblastoma treatment by induction of noptosis, an NQO1-dependent necrosis. *Free Radic Biol Med* 2021;**166**:104−15.
16. Bey EA, Reinicke KE, Srougi MC, Varnes M, Anderson VE, Pink JJ, et al. Catalase abrogates β-lapachone-induced PARP1 hyperactivation-directed programmed necrosis in NQO1-positive breast cancers. *Mol Cancer Ther* 2013;**12**:2110−20.
17. Tagliarino C, Pink JJ, Dubyak GR, Nieminen AL, Boothman DA. Calcium is a key signaling molecule in β-lapachone-mediated cell death. *J Biol Chem* 2001;**276**:19150−9.
18. Kawecki A, Adkins D, Cunningham C, Vokes E, Yagovane D, Dombal G, et al. A phase II study of ARQ 501 in patients with advanced squamous cell carcinoma of the head and neck. *J Clin Oncol* 2007;**25**:16509.
19. Beg MS, Huang X, Silvers MA, Gerber DE, Bolluyt J, Sarode V, et al. Using a novel NQO1 bioactivatable drug, β-lapachone (ARQ761), to enhance chemotherapeutic effects by metabolic modulation in pancreatic cancer. *J Surg Oncol* 2017;**116**:83−8.
20. Dong Y, Morris-Natschke SL, Lee KH. Biosynthesis, total syntheses, and antitumor activity of tanshinones and their analogs as potential therapeutic agents. *Nat Prod Rep* 2011;**28**:529−42.
21. Zhao W, Li B, Hao J, Sun R, He P, Lv H, et al. Therapeutic potential of natural products and underlying targets for the treatment of aortic aneurysm. *Pharmacol Ther* 2024;**259**:108652.
22. Chen X, Guo J, Bao J, Lu J, Wang Y. The anticancer properties of *Salvia miltiorrhiza* Bunge (Danshen): a systematic review. *Med Res Rev* 2014;**34**:768−94.
23. Wang X, Yang Y, Liu X, Gao X. Pharmacological properties of tanshinones, the natural products from *Salvia miltiorrhiza*. *Adv Pharmacol* 2020;**87**:43−70.
24. Ashrafizadeh M, Zarrabi A, Orouei S, Saberifar S, Salami S, Hushmandi K, et al. Recent advances and future directions in anti-tumor activity of cryptotanshinone: a mechanistic review. *Phytother Res* 2021;**35**:155−79.
25. Li H, Gao C, Liu C, Liu L, Zhuang J, Yang J, et al. A review of the biological activity and pharmacology of cryptotanshinone, an important active constituent in Danshen. *Biomed Pharmacother* 2021;**137**:111332.
26. Wu YH, Wu YR, Li B, Yan ZY. Cryptotanshinone: a review of its pharmacology activities and molecular mechanisms. *Fitoterapia* 2020;**145**:104633.
27. Hao W, Zhang X, Zhao W, Zhu H, Liu Z-Y, Lu J, et al. Cryptotanshinone induces pro-death autophagy through JNK signaling mediated by reactive oxygen species generation in lung cancer cells. *Anticancer Agents Med Chem* 2016;**16**:593−600.
28. Xiao Q, Zhong B, Hou Y, Wang M, Guo B, Lin L, et al. Fighting cancer by triggering non-canonical mitochondrial permeability transition-driven necrosis through reactive oxygen species induction. *Free Radic Biol Med* 2023;**202**:35−45.
29. Hou Y, Liu R, Xia M, Sun C, Zhong B, Yu J, et al. Nannocystin ax, an eEF1A inhibitor, induces G1 cell cycle arrest and caspase-independent apoptosis through cyclin D1 downregulation in colon cancer *in vivo*. *Pharmacol Res* 2021;**173**:105870.
30. Vivian JT, Callis PR. Mechanisms of tryptophan fluorescence shifts in proteins. *Biophys J* 2001;**80**:2093−109.
31. Morris GM, Huey R, Lindstrom W, Sanner MF, Belew RK, Goodsell DS, et al. AutoDock4 and AutoDockTools4: automated docking with selective receptor flexibility. *J Comput Chem* 2009;**30**:2785−91.
32. Trott O, Olson AJ. AutoDock Vina: improving the speed and accuracy of docking with a new scoring function, efficient optimization, and multithreading. *J Comput Chem* 2010;**31**:455−61.
33. Pettersen EF, Goddard TD, Huang CC, Couch GS, Greenblatt DM, Meng EC, et al. UCSF Chimera—a visualization system for exploratory research and analysis. *J Comput Chem* 2004;**25**:1605−12.
34. Laskowski RA, Swindells MB. LigPlot+: multiple ligand−protein interaction diagrams for drug discovery. *J Chem Inf Model* 2011;**51**:2778−86.
35. Chen Z, Zhu R, Zheng J, Chen C, Huang C, Ma J, et al. Cryptotanshinone inhibits proliferation yet induces apoptosis by suppressing STAT3 signals in renal cell carcinoma. *Oncotarget* 2017;**8**:50023.

36. Chen W, Lu Y, Chen G, Huang S. Molecular evidence of cryptotanshinone for treatment and prevention of human cancer. *Anticancer Agents Med Chem* 2013;**13**:979−87.
37. Faig M, Bianchet MA, Winski SL, Hargreaves R, Moody CJ, Hudnott AR, et al. Structure-based development of anticancer drugs: complexes of NAD(P)H:quinone oxidoreductase 1 with chemotherapeutic quinones. *Structure* 2001;**9**:659−67.
38. Lee H, Park MT, Choi BH, Oh ET, Song MJ, Lee J, et al. Endoplasmic reticulum stress-induced JNK activation is a critical event leading to mitochondria-mediated cell death caused by β-lapachone treatment. *PLoS One* 2011;**6**:e21533.
39. Douglas DL, Baines CP. PARP1-mediated necrosis is dependent on parallel JNK and Ca^{2+}/calpain pathways. *J Cell Sci* 2014;**127**:4134−45.
40. Lee JY, Kim WK, Bae KH, Lee SC, Lee EW. Lipid metabolism and ferroptosis. *Biology* 2021;**10**:184.
41. Bentle MS, Reinicke KE, Bey EA, Spitz DR, Boothman DA. Calcium-dependent modulation of poly(ADP-ribose) polymerase-1 alters cellular metabolism and DNA repair. *J Biol Chem* 2006;**281**:33684−96.
42. Yu J, Zhong B, Zhao L, Hou Y, Ai N, Lu JJ, et al. Fighting drug-resistant lung cancer by induction of NAD(P)H:quinone oxidoreductase 1 (NQO1)-mediated ferroptosis. *Drug Resist Updat* 2023;**70**:100977.
43. Parkinson EI, Hergenrother PJ. Deoxynyboquinones as NQO1-activated cancer therapeutics. *Acc Chem Res* 2015;**48**:2715−23.
44. Qi P, Li Y, Liu X, Jafari FA, Zhang X, Sun Q, et al. Cryptotanshinone suppresses non-small cell lung cancer *via* microRNA-146a-5p/EGFR axis. *Int J Biol Sci* 2019;**15**:1072−9.
45. Ye T, Zhu S, Zhu Y, Feng Q, He B, Xiong Y, et al. Cryptotanshinone induces melanoma cancer cells apoptosis *via* ROS-mitochondrial apoptotic pathway and impairs cell migration and invasion. *Biomed Pharmacother* 2016;**82**:319−26.
46. Ke F, Wang Z, Song X, Ma Q, Hu Y, Jiang L, et al. Cryptotanshinone induces cell cycle arrest and apoptosis through the JAK2/STAT3 and PI3K/Akt/NFκB pathways in cholangiocarcinoma cells. *Drug Des Devel Ther* 2017;**11**:1753−66.
47. Liu C, Sun HN, Luo YH, Piao XJ, Wu DD, Meng LQ, et al. Cryptotanshinone induces ROS-mediated apoptosis in human gastric cancer cells. *Oncotarget* 2017;**8**:115398−412.
48. Cho MH, Niles A, Huang R, Inglese J, Austin CP, Riss T, et al. A bioluminescent cytotoxicity assay for assessment of membrane integrity using a proteolytic biomarker. *Toxicol Vitro* 2008;**22**:1099−106.
49. Wlodkowic D, Telford W, Skommer J, Darzynkiewicz Z. Apoptosis and beyond: cytometry in studies of programmed cell death. *Methods Cell Biol* 2011;**103**:55−98.
50. Yu J, Zhong B, Xiao Q, Du L, Hou Y, Sun HS, et al. Induction of programmed necrosis: a novel anti-cancer strategy for natural compounds. *Pharmacol Ther* 2020;**214**:107593.
51. Jin X, Jin W, Tong L, Zhao J, Zhang L, Lin N. Therapeutic strategies of targeting non-apoptotic regulated cell death (RCD) with small-molecule compounds in cancer. *Acta Pharm Sin B* 2024;**14**:2815−53.
52. Silvers MA, Deja S, Singh N, Egnatchik RA, Sudderth J, Luo X, et al. The NQO1 bioactivatable drug, β-lapachone, alters the redox state of $NQO1^+$ pancreatic cancer cells, causing perturbation in central carbon metabolism. *J Biol Chem* 2017;**292**:18203−16.
53. Doppler D, Sonker M, Egatz Gomez A, Grieco A, Zaare S, Jernigan R, et al. Modular droplet injector for sample conservation providing new structural insight for the conformational heterogeneity in the disease-associated NQO1 enzyme. *Lab Chip* 2023;**23**:3016−33.
54. Grieco A, Ruiz Fresneda MA, Gómez Mulas A, Pacheco García JL, Quereda Moraleda I, Pey AL, et al. Structural dynamics at the active site of the cancer-associated flavoenzyme NQO1 probed by chemical modification with PMSF. *FEBS Lett* 2023;**597**:2687−98.
55. Bey EA, Bentle MS, Reinicke KE, Dong Y, Yang C-R, Girard L, et al. An NQO1-and PARP-1-mediated cell death pathway induced in non-small-cell lung cancer cells by β-lapachone. *Proc Natl Acad Sci U S A* 2007;**104**:11832−7.
56. Dixon SJ, Lemberg KM, Lamprecht MR, Skouta R, Zaitsev EM, Gleason CE, et al. Ferroptosis: an iron-dependent form of non-apoptotic cell death. *Cell* 2012;**149**:1060−72.
57. Huang X, Motea EA, Moore ZR, Yao J, Dong Y, Chakrabarti G, et al. Leveraging an NQO1 bioactivatable drug for tumor-selective use of poly(ADP-ribose) polymerase inhibitors. *Cancer Cell* 2016;**30**:940−52.